Understanding the Evolution of Miscible Viscous Fingering Patterns

by

Jane Chui

Submitted to the Department of Civil and Environmental Engineering
in partial fulfillment of the requirements for the degree of

Master of Science in Civil and Environmental Engineering

at the

MASSACHUSETTS INSTITUTE OF TECHNOLOGY

September 2012

Author .....
Department of Civil and Environmental Engineering
August 10, 2012

Certified by .....
Ruben Juanes
Associate Professor of Civil and Environmental Engineering
Thesis Supervisor

Accepted by .....
Heidi M. Nepf
Chair, Departmental Committee for Graduate Students

Understanding the Evolution of Miscible Viscous Fingering Patterns

by

Jane Chui

Submitted to the Department of Civil and Environmental Engineering
on August 10, 2012, in partial fulfillment of the
requirements for the degree of
Master of Science in Civil and Environmental Engineering

Abstract

Viscous fingering, the hydrodynamic instability that occurs when a lower viscosity fluid displaces a higher viscosity fluid, creates complex patterns in porous media flows. Fundamental facets of the displacement process, such as volumetric sweep and mixing efficiency, depend strongly on the type of pattern created by the uneven front of the less viscous fluid. The interface created from these fingering patterns affects mixing, and therefore understanding how these patterns evolve is of critical importance in applications such as enhanced oil recovery and groundwater remediation.

We use a Hele-Shaw cell to study experimentally how changing three parameters — the injection rate, the viscosity contrast between the two fluids, and the gap thickness through which the fluid flows — affects the resulting fingering pattern. The results lead to some basic observations, such as finger widths increasing uniformly with gap thickness, or that increasing the mobility ratio leads to more and narrower fingers. However, this systematic experimental method also uncovered an unexpected trend: non-monotonic finger width behavior with respect to injection rate. This non-monotonicity was observed for all mobility ratios and gap thicknesses, and is summarized in the experimental phase diagram created.

To further understand how a viscous fingering pattern evolves over time, we also calculate the interface growth of a pattern over time using image analysis. This analysis shows that the interface moves through three self-similar regimes over time, and suggests that viscous fingering only actively adds interfacial length for a certain period of time in a pattern's growth.

Both of these findings impact how much interfacial area a fingering pattern can create, and developing a better understanding of the evolution of miscible viscous fingering patterns is necessary for being able to accurately determine the mixing efficiency of a fingering pattern.

Thesis Supervisor: Ruben Juanes
Title: Associate Professor of Civil and Environmental Engineering

Acknowledgments

I would first and foremost like to thank my research advisor Ruben Juanes, whose dedication, brilliance, and kindness inspires me to do my best every day. I have learned so much since I started, and I am sure that I will continue to do so under your guidance.

I would like to then extend my deepest gratitude to Mike Szulczewski, who has been instrumental in every single thing I have attempted since my arrival here at MIT. Thank you so much for your help, guidance, advice, and patience; I appreciate most the time that you freely carve out of your day to help me when I find myself in the weeds, which happens more often than I would like to admit.

I would of course like to thank everyone in the Juanes Research Group. Thank you for all the ideas and advice when I've been stuck. I would especially like to thank Chris MacMinn and Birendra Jha. Chris, in addition to answering all of my research questions, thank you for helping me with anything and everything computer-related. My conversion to Apple would not have been complete without you. Birendra, thank you for being so helpful, patient, and knowledgeable in all things numerical.

No list of thanks would be complete without thanking the wonderful people who keep the smile on my face every day and who never hesitate to help with all the little things, not to mention all the big things. Thus, a big thank you to all of my friends and colleagues. I would also like to thank Kris Kipp, Patty Glidden, Sheila Frankel, and Jim Long — life would be so much harder without your tireless work behind the scenes.

Finally, I would like to dedicate this work to my amazing family. Thank you so much for your unconditional love, support, and encouragement, and support from day one. I hope I continue to make all of you proud.

Contents

List of Figures

Chapter 1

Introduction

Viscous fingering is a hydrodynamic instability that occurs when a less viscous fluid displaces a more viscous one. Instead of progressing as a uniform front, the less viscous fluid forms fingers that vary in size and shape to create complex patterns. The complex patterns created are relevant in applications such as enhanced oil recovery and bioremediation because they affect the volumetric sweep and mixing efficiency.

Depending on the application being discussed, viscous fingering can be an aid or a hindrance, and this can be illustrated using the two properties already mentioned. Volumetric sweep refers to how much of the defending fluid is displaced, and so a uniform front would have the largest volumetric sweep possible. In the context of viscous fingering, the amount of untouched volume left between the fingers will affect the volumetric sweep, and this untouched volume will depend on the spacing and size of the fingers. The mixing efficiency, on the other hand, is related more closely to the interfacial length created between the two fluids, as this will facilitate mixing. In enhanced oil recovery, the goal is to increase the volumetric sweep as much as possible because the injected fluid will displace the oil in the reservoir, and so in general less fingers is beneficial. This is not the case in bioremediation, however, as contaminants are often sorbed to the soil and the bacteria suspension or nutrients being injected is intended for delivery and and not displacement. The existence of more fingers actually can help with creating more interfacial area over which bacteria can come

into contact with the contaminants.

Whether the fingering patterns are desired or not, these patterns impact applications such as oil recovery, and so they need to be understood. Although viscous fingering has been studied for many years, the effect of parameters such as the viscosity ratio and the injection rate on the evolution of viscous fingering patterns remains poorly understood.

1.1 Objectives

While viscous fingering occurs with both miscible or immiscible fluids, here we focus on miscible displacements. We study these displacements in a radial geometry as a proxy for the point-source injections common to applications such as enhanced oil recovery.

There are two key objectives to this research. The first objective is to understand how fingering patterns evolve as key parameters — injection rate, pore size, and viscosity ratio between the two fluids — are changed. The goal is to experimentally map out a detailed phase diagram that demonstrates the trends and effects these parameters have on the fingering pattern. The second objective is to understand how fingering patterns evolve over time. The interfacial length across which mixing can occur changes over time, and understanding this is important in determining the mixing efficiency of a particular pattern.

1.2 Previous Work

Viscous fingering has been extensively studied, especially in the context of oil recovery. Consisting of two parallel plates with a thin fluid-filled gap in between, the Hele-Shaw has been used as a porous media analog by many researchers to investigate viscous fingering patterns [6, 8, 15]. For miscible displacements, water and glycerol are the

two most common fluids used [8] and they are the fluids used in this research as well.

There are many numerical studies that model radial fingering behavior [2, 1], but only a handful of experimental studies, and they consider a range of issues, from fractal patterns that emerge [13] to stability and onset questions [4, 7]. From this subset of experimental studies dealing with radial miscible fingering, there are only a few that focus experimentally on characterizing the actual patterns of viscous fingering. In these experiments, the dominant wavelength of a fingering pattern, which is essentially twice the finger width of an average finger, is the main emphasis. Among these studies, however, there are inconsistencies mainly due to the fact that each investigator has sampled only a small subset of parameters. The following are three examples:

Paterson (1985) concluded that finger width is not a function of injection rate, but a function of gap thickness in the Hele-Shaw cell [10]. Thus, if the gap width was increased, the finger width will increase as well. However, as he noted himself, he was only able to investigate a very limited range of flow rates that span a factor of five. Higher flow rates caused flexing, and slower flow rates did not finger within the physical confines of the Hele-Shaw cell that was used. The gap thicknesses used varied by a factor of two, as there were issues with the flatness of the plates [10]. They could not be increased because the gap was already quite large (1.5 and 3 mm) and towards the high end of gap thicknesses over which the Hele-Shaw approximation as a porous media flow would apply.

In Chen's work in 1987 [3], a similar conclusion was reached. He concluded that flow rate only had a weak influence on fingering patterns for miscible fluids. He noted instead that a larger influence was observed on immiscible fluids. where an increasing flow rate resulted in more fingers, and fingers that were narrower. Both Paterson's and Chen's experiments used pure glycerine and water as fluids, and water was injected in the center of the Hele-Shaw cell. However, the gap thickness was much smaller at 75 microns, and the velocities tested also had a larger range, varying from 0.008mL/min

to 0.12 mL/min, which is just over one order of magnitude of range.

In a slightly different configuration in which a circular spot of fluid was displaced by fluid moving past it, the conclusion was very different. In these studies, the " tail" or the fluid from the circular spot that was dispersed, fingers into the surrounding fluid, much in the same way a constant injection of a less viscous fluid would finger as it is pushed into the more viscous one. In these experiments, it was noted that for increasing Péclet numbers, there are more and also narrower fingers [11]. The Péclet number was defined in this work as $Q/(2\ \pi\ D)$, and since the diffusion coefficient (D) was constant, an increase in the Péclet number translates to an increase in the injection rate (Q). Here the gap thickness was kept constant at 610 microns, in between the thicknesses of the two studies previously mentioned. A key difference in this study was that instead of pure glycerol, water-glycerol mixtures were used as the defending fluid in some of the runs, and so the viscosity ratio ranged from 3 to 153 [11].

It is evident that these are results that exist in diiferent regions of the parameter space, and there is currently no work that bridges the gap between these studies and others similar to them. More importantly, there is no study that investigates how radial miscible fingering patterns change. Since the previous work discussed here has indicated, albeit separately, that the parameters of gap thickness, injection rate, and viscosity ratio can all influence the finger widths, there is motivation to conduct a systematic experimental search of when and how these parameters apply to radial miscible viscous fingering patterns.

Chapter 2

Laboratory Experiments

2.1 Rationale

As demonstrated in the literature review in the previous section, there is currently a lack of experimental data in the area of radial miscible viscous fingering. There is experimental data for certain specific cases, but there is no continuous data that systematically investigates how fingering patterns evolve over time for different parameters. In addition, much of the computational work in this area can benefit from comparisons made to experimental results.

The experimental work presented here seeks to fill this void systematically, with the aid of image analysis. A radial Hele-Shaw cell will be used as an analog to porous media flow, and the parameters of viscosity ratio, displacement rate, and pore size will be studied through varying the viscosities of fluid pairs, changing injection rates, and changing the gap thickness of the Hele-Shaw cell respectively. Analysis of differences in fingering patterns via attributes such as interface length and average finger width will map out the evolution of these patterns.

2.2 Experimental Method

2.2.1 Hele-Shaw Apparatus

The Hele-Shaw cell used in these experiments is created with two circular pre-fabricated pieces of borosilicate glass, measuring 21.275 cm (8-3/8 in) in diameter and 1.9 cm (3/4 in) in thickness. The gap thickness of the Hele-Shaw cell is created by the placement of a set of precision shims between the two glass plates. Eight of these shims are spaced equidistantly around the perimeter, and clamps are applied in the same configuration as the shims to hold the entire Hele-Shaw cell together.

This Hele-Shaw cell is distinct from Hele-Shaw cells common in previous research as it has separate injection ports for the defending (more viscous) and invading (less viscous) fluids. The separate injection ports ensure that the two fluids remain intact prior to entering the Hele-Shaw cell and that no mixing occurs to change the viscosity of either fluid. This is important because the viscosity contrast between the two fluids becomes an unknown, and repeatability is questionable. The inlets are two circular holes drilled into the center of each glass disc, and a connection port leads tygon tubing to the two syringes that hold the invading and defending fluids. A syringe pump controls the injection rate of the invading fluid, and the volumetric flow rate is kept constant for each experiment.

2.2.2 Injection Rate Considerations

There are two limits to the range of injection rates that can be used, and the lower and upper limits are the physical limits of the syringe pump itself and the strength of the glass plates respectively. The slowest that the syringe pump can reliably inject depends on the size of syringe used, and for the set-up used in this set of experiments, the lowest injection rate is 0.002 mL/min. The upper limit depends on the strength of the plates because once the glass plates deflect a significant amount, the gap is no longer uniform and the apparatus can no longer be considered a Hele-Shaw cell

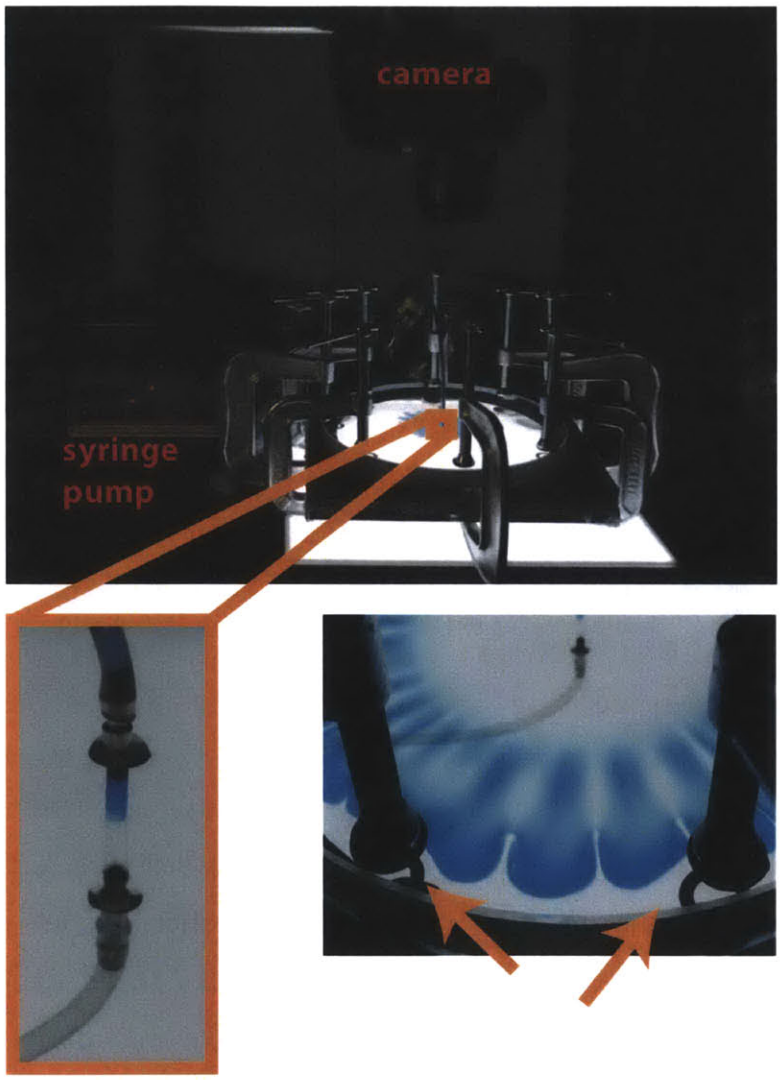

Figure 2-1: Hele-Shaw Apparatus: This is the experimental set-up used to collect all of the data discussed here. The camera is mounted directly overhead the Hele-Shaw cell while an LED light panel provides luminescence from below. A syringe pump controls the rate at which the invading fluid, dyed blue, enters the Hele-Shaw cell. On the lower left is a magnification of the two-port design of this Hele-Shaw cell, while on the lower right the precision metal shims can be seen clamped in between the two glass plates. This creates the desired gap thickness in the Hele-Shaw cell.

because the plates are not parallel. It will also be hard to determine whether the changes in fingering pattern is due to the parameters being changed or the deflection of the cell. Thus, it was necessary to determine whether the deflection fraction of the plates caused by pressures from fluid injected at high velocites will be significant. For this, we can use a deflection formula developed for circular, parallel plates that have constant pressure applied over the entire surface [17]:

$$\Delta = \frac{-9}{4 * \pi} * \frac{Q * \mu_h * R^4}{E * t^3 * b^4} \tag{2.1}$$

where

μ_h = viscosity of more viscous fluid [Pa s]

R = radius of Hele-Shaw cell [m]

E = Young's modulus for glass (=2$\times$ 10^9) [Pa]

t = thickness of glass plate [m]

Q = injection rate $[m^3/s]$

b = gap thickness [m]

However, because we know that the pressure is in actuality highest at the injection port as that is where the fluid has the highest velocity, the deflection fraction will be an over-estimate if we assume the force applied at the injection port was applied over the entire cell. Even with this assumption, it was determined that the injection rates investigated for this set of experiments, ranging from 0.002 mL/min to 2 mL/min, cause insignificant deflection in the glass plates.

2.2.3 Gap Thickness Considerations

In determining the minimum gap thickness possible in this Hele-Shaw cell, the tolerance in thickness of the metal shims and the smoothness of both glass plates have to be taken into account. Otherwise, the gap will not be even across the entire cell. As mentioned in Section 1.2, this was why in previous work researchers were unable to test a larger range of gap thicknesses in their experiments [10]. The metal shims

used here have a tolerance of ± 7.62 μm (0.0003 in), so any of the available precision shim stock (the thinnest is 25 microns) will not be the limiting factor in selecting a gap thickness. This leaves the scaling of any possible warping or irregularities in the glass to determine the minimum gap thickness. Since any irregularities in glass smoothness of the two bounding plates will be on the micron scale, simple inspection by naked eye is not sufficient. Thus, a radial expansion test is performed to ensure that the smoothness of the glass will not interfere with the creation of a uniform gap using the precision shims. For the radial expansion test, two preparations of the same fluid is used — one dyed and one undyed. Being of the same viscosity, the invading fluid should expand uniformly. If the expansion is not circular, then there are irregularities within the gap that are influencing the expansion. In this manner, starting with the thinnest precision shim, it was determined experimentally that the smallest gap possible using these materials would be 50 microns. In the experiments discussed in the next section, three different gap thicknesses were used: 50 μm, 100 μm, and 200 μm.

2.2.4 Viscosity Considerations

To create fluids of varying viscosities, different combinations of glycerol and water are used. Water is used as the base fluid in this experimental system, and as such is used as the invading fluid in all runs of the experiments discussed in this thesis. To avoid variations in density and solubility between runs of the experiment due to variations in the chemical make-up of tap water, milli-Q water — a highly purified water clear of trace organics, metals, and other impurities — is used instead for both the base fluid and the solvent for the higher viscosity fluids. The higher viscosity fluids are created by dissolving specific amounts of glycerol into water, as per the mass fractions calculated using formulas developed empirically by fitting curves to experimental data [5]. It is a recursive process to determine the exact mass fraction glycerol that needs to be added to water. The two input parameters are temperature and mass fraction of glycerol. The temperature is used to calculate the dynamic viscosity of both pure

water and pure glycerol using the following equations:

$$\begin{aligned} \mu_{water} &= 1.790 * e^{\frac{(-1230-T)*T}{36100+360*T}} \\ \mu_{glycerol} &= 12100 * e^{\frac{(-1233+T)*T}{9900+70*T}} \end{aligned} \tag{2.2}$$

where μ is the viscosity and T is the temperature in Kelvin. The parameters, a and b, are calculated using the following relationships:

$$\begin{aligned} a &= 0.705 - 0.0017 * T; \\ b &= (4.9 + 0.036 * T) * a^{2.5}; \end{aligned} \tag{2.3}$$

and in combination with the mass fraction of glycerol, represented by parameter c, the partition coefficient α is calculated. This partition coefficient is then used to calculate the dynamic viscosity (in centiPoise) of the glycerol-water mixture:

$$\alpha = 1 - c + frac(a * b * c * (1 - c))(a * c + b * (1 - c)); \tag{2.4}$$

$$\mu_{mixture} = \mu_{water}^{\alpha} * \mu_{gly}^{(1-\alpha)} \tag{2.5}$$

This has to be repeated until a mass fraction of glycerol is estimated correctly to give the desired viscosity. The mass fractions of glycerol used to create fluids that are 2, 5, and 10 times more viscous than water are 0.222, 0.451, and 0.576 respectively.

2.2.5 Density Considerations

Since adding glycerol changes the density of the fluid, it is necessary to ensure that gravity will not be an added parameter affecting the results, even though the Hele-Shaw cell is oriented horizontally and gravity affects the entire cell evenly. The highest density difference occurs for the fluid ten times more viscous than water, and it is approximately 15% more dense than water. To ensure that gravity is not affecting the fingering patterns observed and especially not the onset of fingering, the gravity number is calculated to determine whether gravity is a negligible parameter

in this system. The gravity number (Gr) is defined as:

$$Gr = \frac{\text{time for advection}}{\text{time for tip of finger to deflect}} \tag{2.6}$$

which after simplification works out to be:

$$Gr = \frac{g * (\rho_h - \rho_l) * b^3 * r_{fing}}{(\mu_h * Q)} * \frac{\pi}{6} \tag{2.7}$$

where

ρ_h = density of more viscous fluid [kg/m^3]

ρ_l = density of less viscous fluid [kg/m^3]

r_{fing} = radius at which fingering starts [m]

μ_h = viscosity of more viscous fluid [cP]

Q = injection rate [m^3/s]

g = acceleration due to gravity, 9.81 [m/s^2]

Systems in which it takes a much longer time for the finger to deflect than it takes for the finger to travel a distance away from the injection port, have a gravity number that is much less than one. These systems are deemed to be systems in which gravity is not a controlling parameter. For the range of parameters used in all of the experiments discussed here, the gravity number is much lower than one, and the highest is still in the tenths. Thus, gravity is neglected in the interpretation of the experimental results discussed in this work.

2.2.6 Imaging Considerations

Imaging of the fingering patterns is done via a camera mounted with the center of the lense directly above the center of the Hele-Shaw cell. A light panel illuminates the cell from below, and for visualization purposes, the invading fluid (water) is dyed with eriogluacine (blue food coloring) at a concentration of 0.01mg/mL. Because the intensity of colour visible correlates directly with the amount of tracer the light passes

through, the dyed fluid will appear lighter in experiments conducted at a smaller gap thickness than those conducted at a larger one. Thus, this concentration was chosen because the dyed fluid is still easily distinguished from the defending fluid at the smallest gap thickness of 50 microns. It is important to use the lowest possible visible concentration of erioglaucine because the molecule itself is large with a molecular weight of 792.85 g/mol [16], and can impact the density of the invading fluid itself. At this concentration, the added mass of tracer is negligible and the tracer remains passive in that it does not change the density of the fluid itself.

Chapter 3

Results and Discussion

The results discussed in this chapter are from a set of experiments in which three parameters — the injection rate (Q), the mobility ratio (M), and the gap thickness (b) — are varied. The constant volume injection rate varies between 0.002 mL/min and 2 mL/min, and refers to the injection of the less viscous invading fluid into the Hele-Shaw cell. The ratio of viscosities of the defending fluid to the invading fluid is referred to as the mobility ratio. For this set of experiments, the range of mobility ratios investigated is from $M = 2$ to $M = 10$, with a subset of control experiments conducted at $M = 1$, which refers to the case in which the invading and defending fluids are of the same viscosity and no fingering should be expected. Finally, three unique gap thicknesses are used: 50, 100, and 200 microns.

For each combination of the three parameters tested, the experiment was run a minimum of three times to ensure repeatability, and the field of view of the overhead camera recording the experiment was kept constant so that properties that involve scaling, such as finger width, can be compared directly between experiments. It should be further noted that for comparison purposes, the radial distance away from the injection port was used to normalize the images that are included here.

Thus, the total volume of fluid injected and the time stamp of the images of different experiments being compared will vary, but the scale is the same. Each fingering pattern image is therefore representative of a 9.5cm $\times$ 9.5cm window of the Hele-Shaw cell, viewed from above the cell.

3.1 Basic Observations

The following is a summary of some basic observations that emerge as trends in the fingering pattern as one parameter is changed while others are kept constant.

3.1.1 Control Experiments

We must confirm that the tracer chosen for visually differentiating between the invading and defending fluids does not affect the properties of the fluid. In other words, we need to confirm that the tracer is indeed a passive tracer. The invading fluid for the entire set of experiments is Q-water dyed blue with 0.01 g/mL of erioglaucine, also known as blue food coloring. For all gap thicknesses and for all injection rates, a solid circle with a uniform front is observed for the control case of $M = 1$ (Fig. 3-1).

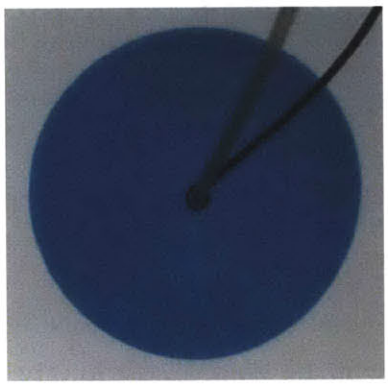

Figure 3-1: Radial expansion is observed for all of the control cases in which the mobility ratio is 1, where both fluids are water and the invading fluid is dyed blue.

This confirms that the erioglaucine used at this concentration is passive, and that the Hele-Shaw cell is radially balanced (i.e. the fluid does not preferentially travel to a certain section of the cell due to pressure imbalances from clamping).

3.1.2 Varying the Mobility Ratio

Having confirmed that equal viscosity fluids do not finger into each other, a set of experiments were completed at different mobility ratios. Keeping both the gap thickness and the injection rate constant, it was observed that increasing the mobility ratio decreases the finger width, which subsequently leads to more fingers and subsequently more complexity at a given distance away from the injection point (Fig. 3-2). Tip-splitting, a phenomenon in which the initial stage of fingers split into two or more new fingers [8], can also be observed at higher mobility ratios.

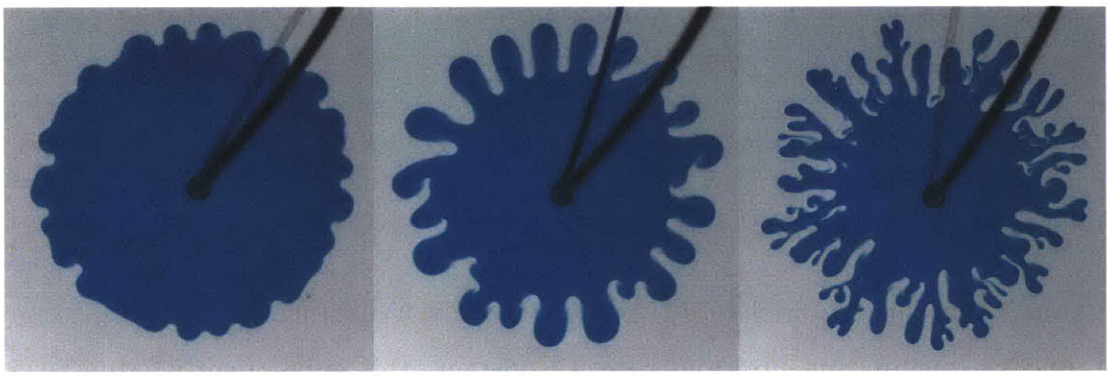

Figure 3-2: This trio of images show how the fingers become thinner and how the pattern becomes more complicated with tip-splitting as the mobility ratio increases. In this series of images, the injection rate is constant at 0.01 mL/min and the gap thickness is set at 50 μm, while the mobility ratio is $M = 2$ (left), $M = 5$ (middle), and $M = 10$ (right).

It can also be observed that the lower the mobility ratio is, the larger the compact core in the resulting fingering pattern at a fixed distance away from the injection point. This is consistent with the observations made in the control experiments in the previous section, where the entire experiment is essentially a compact core. Thus, for mobility ratios close to unity, the closer the ultimate fingering pattern will resemble simple radial expansion. This can be seen in the $M = 2$ case shown on the left in Figure 3-2; the fingers are short and the overall pattern has a large compact core.

3.1.3 Varying the Gap Thickness

Increasing the gap thickness should have a large effect on the overall fingering pattern because for the same radial distance away from the injection point, more volume is required to fill the gap.

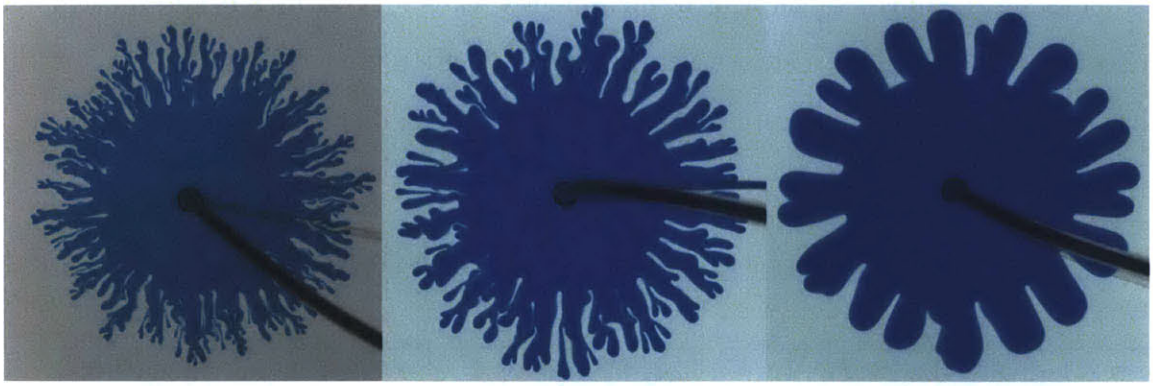

Figure 3-3: This trio of images show how the fingers become thicker and how the pattern becomes less complex as the gap thickness increases. In this series of images, the injection rate is constant at 0.1 mL/min and the mobility ratio is fixed at $M = 5$, while the gap thickness is 50μm (left), 100μm (middle), and 200 μm (right).

Since more volume is required to fill the gap at a given distance from the injection point, and the volumetric injection rate is constant, this subsequently leads to a decrease in the effective velocity of the invading fluid. The larger the gap thickness, the slower the effective velocity, and subsequently the thicker the fingers in the pattern that forms (Fig. 3-3).

3.1.4 Varying the Injection Rate

Changing the constant volume injection rate for a Hele-Shaw cell of fixed dimensions and fluids of fixed mobility will directly change the time it takes for the experiment to complete. Completion is defined as when the fingering pattern expands beyond the 9.5cm $\times$ 9.5 cm viewing window mentioned at the beginning of the chapter. Thus, the higher the injection rate, the less time the experiment takes, and the experimental time lengths for the results shown in Figure 3-4 range from approximately 12 hours for the $Q = 0.002$ mL/min run to less than 20 seconds for the $Q = 2$ mL/min

run. This very short time is important to note because of the appearance of the fingers at high injection rates. There is a halo-like feature around the fingers of patterns created at high injection rates, and although explaining the cause of this is part of the future work mentioned in Section 4.2, knowing the time scale of the experiment excludes diffusion as a possible explanation. Unlike the previous two

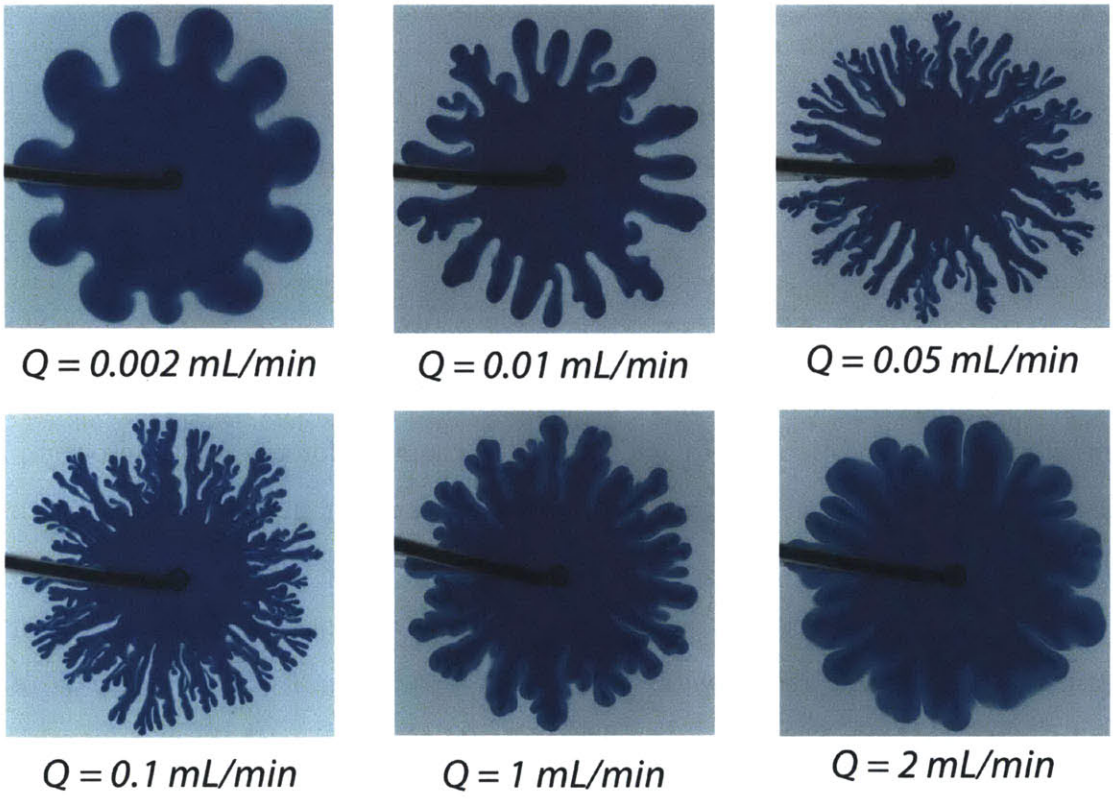

Figure 3-4: This series of images demonstrate how the fingering pattern changes as the constant volume injection rate is increased while keeping the mobility ratio fixed at $M = 10$ and the gap thickness fixed at 100 microns. From $Q = 0.002$ mL/min to $Q = 0.1$ mL/min, the finger widths decrease as the injection rate increases, but from there to $Q = 2$ mL/min, the fingers become wider again.

parameters, the behavior associated with an increasing constant volume injection rate is non-monotonic. Instead of a constantly decreasing finger width in the fingering pattern as the injection rate increases, an inflection point occurs at around 0.1 mL/min, and the finger thinning reverses to have wider fingers as the injection rate continues to increase. This inflection point changes depending on the mobility ratio

and the gap thickness of the Hele-Shaw cell, but is observed for all combinations tested. For example, the inflection occurs at approximately 0.5 mL/min for the case where the mobility ratio is at $M = 5$ and the gap thickness is 50 microns. In this particular combination of parameters, fingers get thinner as the injection rates get closer to 0.5 mL/min, but then get wider at rates faster than 0.5 mL/min. This nonmonotonic behaviour will be discussed further in Section 3.2.1.

3.2 Viscous Fingering Phase Diagram

Having made the basic qualitative observations in the previous section, it is helpful to synthesize all of these findings in a phase diagram, which is a visual map of fingering patterns that allows for comparison across parameters. In both the phase diagram for the 50 micron gap (Figure 3-5) and the phase diagram for the 100 micron gap (Figure 3-6), we observe clearly the non-monotonic behavior in finger widths with respect to injection rates across all mobility ratios. We also observe that for all injection rates and gap thicknesses tested, the compact core of the fingering pattern decreases with increasing mobility ratio. This decreasing compact core is a part of the more complex fingering pattern composed of thinner fingers that emerges with increasing mobility ratio.

The phase diagram validates that all of the trends previously discussed in Section 3.1 apply across the entire range of the parameters tested. Apart from this, we can note that there is a larger difference in the overall fingering pattern between the $M = 2$ and $M = 5$ series of experiments than between the $M = 5$ and the $M = 10$ series of experiments. This can be seen most clearly in Figure 3-5, where the $M = 2$ fingering pattern is very different from the $M = 10$ fingering pattern for each injection rate. In contrast, although there are still differences between the $M = 5$ and $M = 10$ series of experiments according to the trends for increasing mobility ratio previously discussed, the overall fingering patterns of these two series of experiments are very similar.

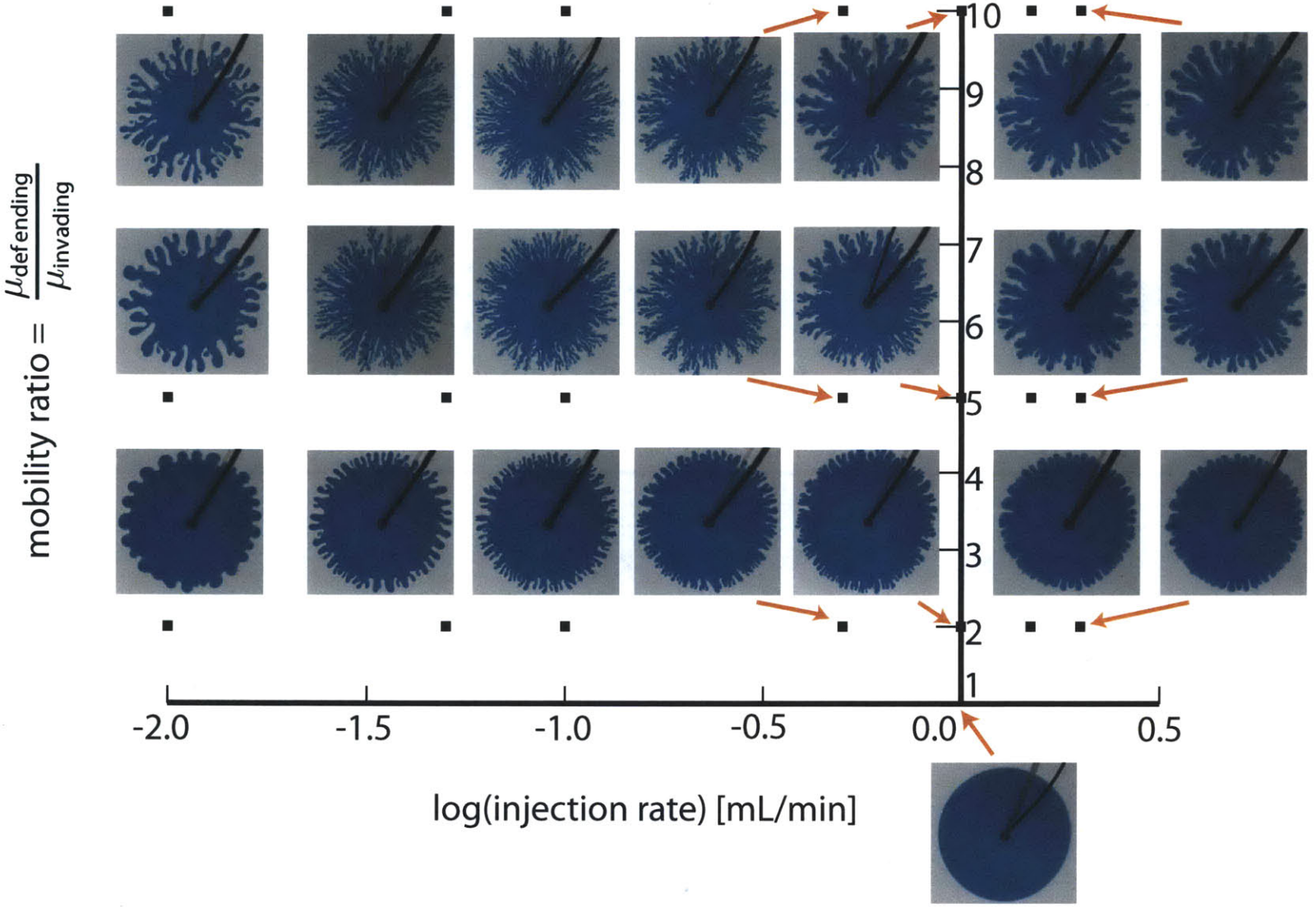

Figure 3-5: Experimental phase diagram of fingering patterns for a 50 micron gap radial Hele-Shaw cell. As can be seen by the images for the $M = 2$ row, viscous fingering occurs as long as there is a viscosity difference. We can see the trends mentioned in the previous section clearly in this diagram, such as observing patterns of increasing complexity with increasing viscosity difference, as well as the non-monotonic finger widths across the different injection rates tested.

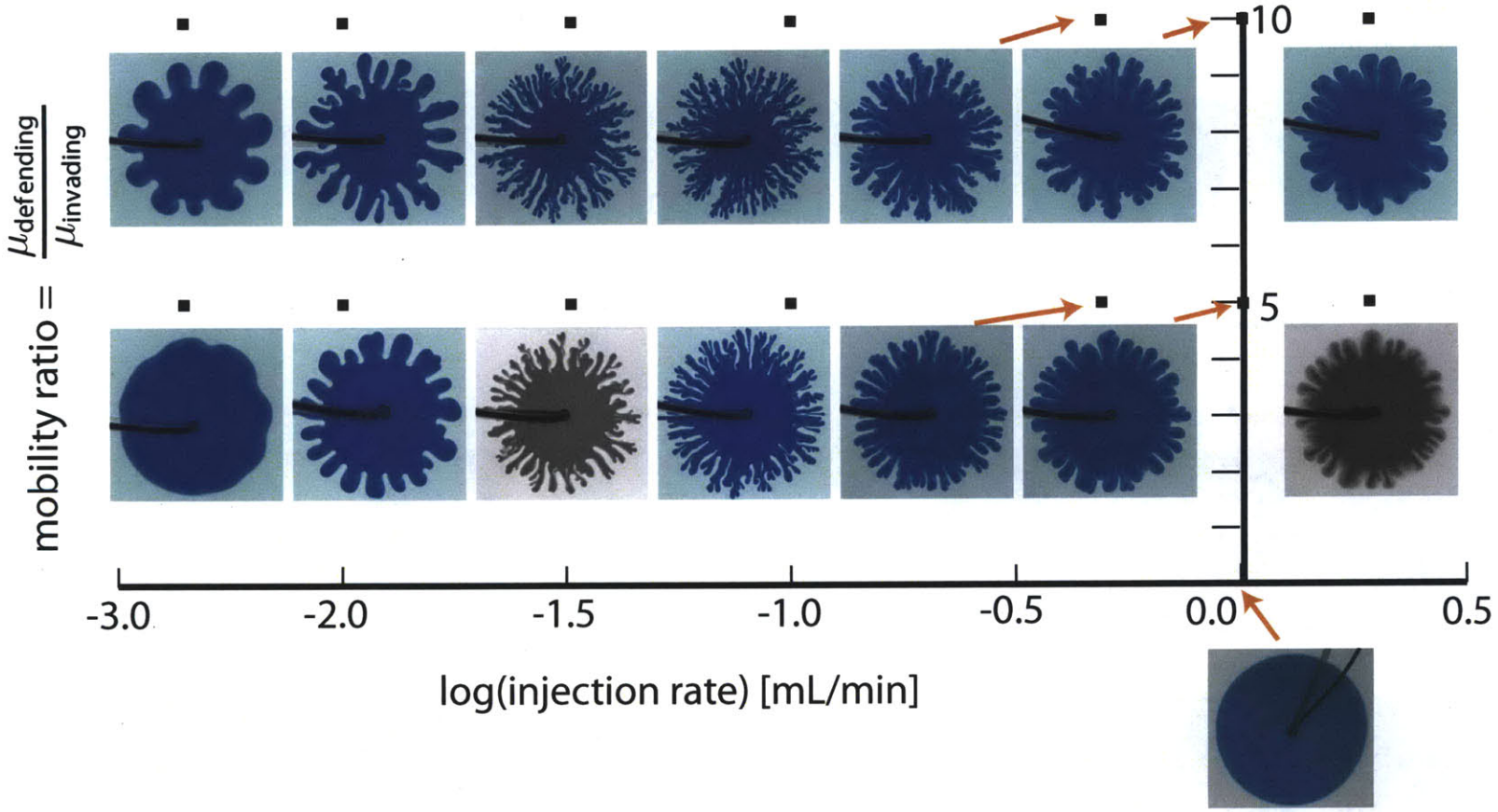

Figure 3-6: Experimental phase diagram of fingering patterns for a 100 micron gap radial Hele-Shaw cell. The non-monotonic behaviour across different injection rates can be observed easily in both the $M = 5$ and $M = 10$ series, and all of the patterns in the $M = 5$ series have a larger compact core than the corresponding images for the same injection rate in the $M = 10$ series.

3.2.1 Linear Stability Analysis

The observed non-monotonicity in finger width with respect to injection rates is unexpected, and so we compare the results with those from a linear stability analysis [14]. According to the linear stability analysis used for this comparison, the most dangerous wavenumber k, defined as

$$k = \frac{2\pi}{\lambda}, \tag{3.1}$$

where λ is the dominant wavelength, increases uniformly as the Péclet number (Pe) increases. The Péclet number is defined as

$$\text{Pe} = \frac{Q}{bD} \tag{3.2}$$

where

Q = injection rate $[m^3/s]$

b = gap thickness [m]

D = diffusion coefficient between the two miscible fluids $[m^2/s]$.

Thus, the dominant wavelength (λ) of a fingering pattern is expected to decrease with an increasing Péclet number. The Péclet number can increase either via an increasing injection rate, Q, or a decreasing gap thickness, b. The diffusion coefficient, D, between the invading and defending fluids changes as the miscible fluids mix into one another, causing a change in the viscosity of the fluids. However, because the diffusion coefficient between glycerol and water is very small, we assume the viscosity of the two fluids to be constant for the duration of the experiment, which results in a constant diffusion coefficient. The fluid viscosity, and subsequently the diffusion coefficient, is also assumed to be constant in the linear stability analysis [14].

To calculate the dominant wavelength from the experimental data, we assume that

$$\lambda = \frac{2\,\pi\,r}{N_f} \tag{3.3}$$

where

N_f = number of fingers

r = radial distance from source injection [m].

Equation 3.3 is simply the perimeter of a bounding circle of radius, r, divided by the number of fingers in the fingering pattern. This arises from assuming that the wavelength, λ, of the pattern is twice the width of a finger. The bounding circle is simply the largest circle that can circumscribe the fingering pattern at a given point in time. Figure 3-7 shows pictorially the two parameters, the wavelength and the bounding circle radius, that are obtained from each fingering pattern to calculate the most dangerous wavenumber needed to compare to the linear stability analysis.

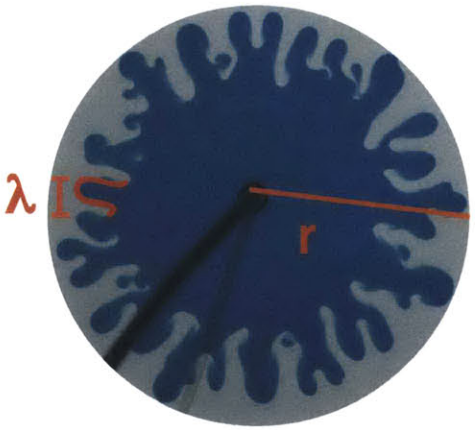

Figure 3-7: This diagram shows the features being measured to obtain the most dangerous wavenumber of a fingering pattern using Equation 3.4. The key assumption here is that one finger width is equal to half the wavelength λ.

When we combine Equation 3.3 with Equation 3.1, we have

$$k = \frac{N_f}{r} \tag{3.4}$$

Using Equation 3.4, we calculate the most dangerous wavenumbers of our experiments at three different fixed radii (r= 2, 3, and 4 cm from the injection point), and plot this versus the Péclet number in Figure 3-8, alongside the results from the linear stability analysis conducted by Riaz and Meiburg in 2003 [14]. We use the gap thickness as the characteristic length for the Péclet number calculation, as this is the characteristic length identified in the linear stability analysis. The analysis sets the Péclet number numerically and so there is no explicit diffusion coefficient that was used, but for our experimental data, we use a value of 10^{-10} m^2/s, an accepted value for water-glycerol mixtures [12]. We see in the resulting Figure 3-8 that there are two distinct sets of data with no overlap. The linear stability analysis yields a mono-tonic linear increase in wavenumber with increasing Péclet number, whereas the wavenumber for the experimental data exhibits non-monotonic behavior with increasing Péclet number at all three radii.

Apart from the difference in behavior, it can also be seen clearly in the figure that there is a disparity in the range of Péclet numbers probed. The analysis by Riaz and Meiburg investigated Péclet numbers from 1 to approximately 10^4, but all of the experimental data had Péclet numbers larger than 10^4. However, it is difficult to reconcile the two very different ranges of Péclet numbers, because numerically large Péclet number simulations are computationally intensive, while small Péclet number experiments are difficult due to limitations in the ranges permitted in either decreasing the injection rate or increasing the gap thickness. It is unclear whether experiments conducted at a lower Péclet number will lose the non-monotonicity or a higher Péclet number linear stability analysis will yield results that agree with the current experiments, but it should be noted that the linear stability analysis had wavenumbers that were much larger than the maximum dangerous wavenumber obtained experimentally.

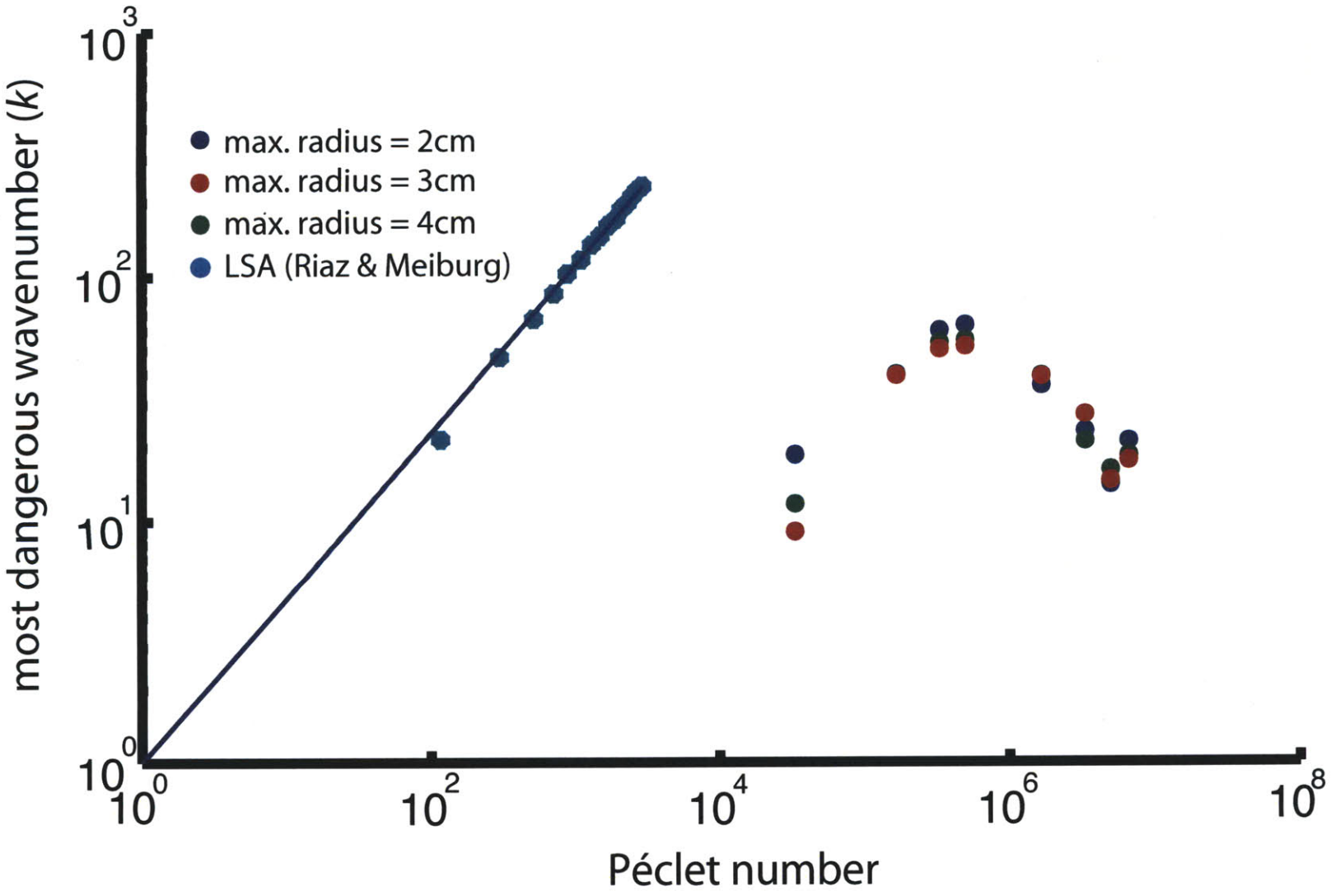

Figure 3-8: The most dangerous wavenumbers are calculated from experimental data at three fixed radii (2, 3, and 4 cm from the injection point) and plotted versus the calculated Péclet number (see Section 3.2.1 for calculation details). The linear stability analysis (LSA) of Riaz and Meiburg [14] is included for comparison. We observe that the wavenumbers calculated from experimental data behave non-monotonically with Péclet number, and are consistent for all three radii. This does not match the wavenumbers of the LSA that exhibit a monotonic increase with Péclet number. However, it should be noted that the experimental data is in an entirely different section of the graph due to the high Péclet numbers generated by using such a small gap thickness (100 microns).

3.3 Quantitative Analysis of Interface Length

3.3.1 Image Processing

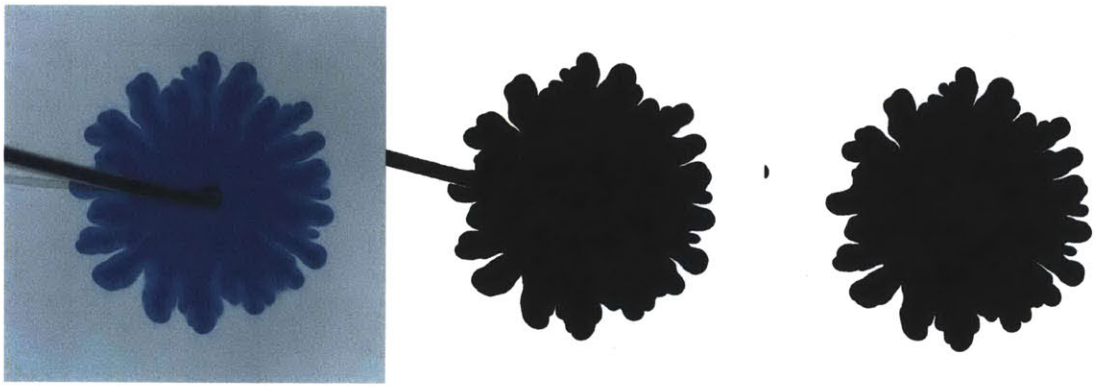

Figure 3-9: This series of images demonstrates how the fingering pattern was processed prior to analyzing its interface length. Starting from the left, the first picture is the raw data image, which is then converted to a black and white image. Finally, it is processed once more using built-in Matlab software to remove the tubing so that the interface length is not skewed by the boundary of the tube.

Since mixing is such a large part of the motivation for research in viscous fingering, investigating the interface length is crucial as this will impact the mixing efficiency of these complex patterns [9]. In this work, the interface length of a fingering pattern is investigated over the duration of the experiment as it grows and evolves.

The Matlab image processing toolbox is used to quantify the interface length of these patterns. The raw photos are converted to binary images using color thresholding. During this process, it is necessary to make use of a removal and interpolation function in Matlab, which first removes the tube and then adequately fills back enough of the image using the surrounding data. In this manner, a time sequence of images were processed to generate a growth curve of interface length over time.

As can be seen in Figure 3-10, the experimental results for data processed for the $M = 2$, $M = 5$, and $M = 10$ cases show that the interface growth rate exhibits three different regimes:

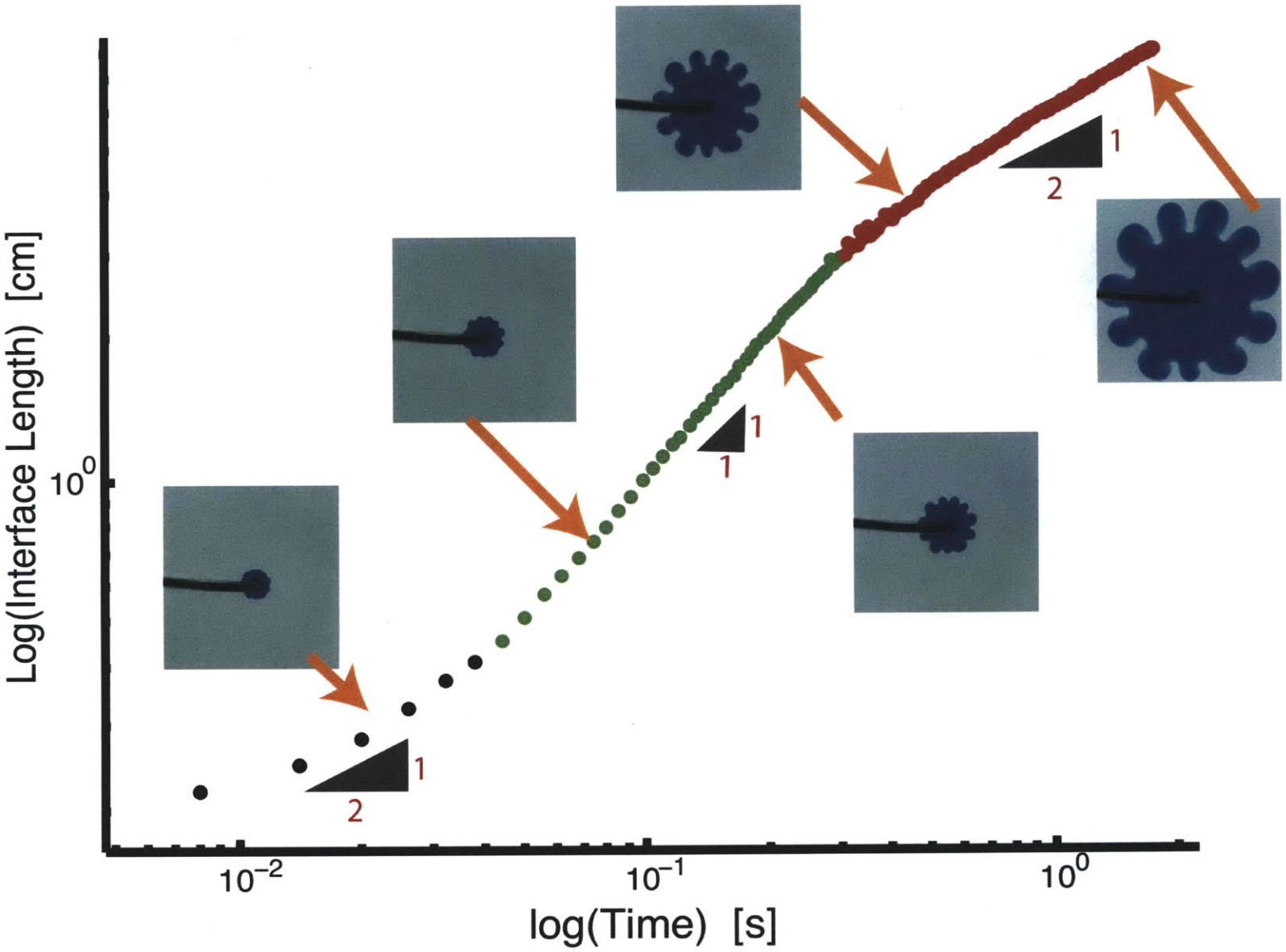

Figure 3-10: The interface length of a fingering pattern moves through three regimes, which are characterized by the changes in the power-law between total interface length and time. The three regimes are: radial expansion (black), accelerated interface growth due to fingering (green), and radial expansion (red). This fingering pattern is created from an injection of fluid ten times less viscous than the defending fluid at a rate of 0.002 mL per minute.

1) Compact radial expansion before fingering
2) Accelerated growth of interface length due to fingering
3) Radial expansion with fixed fingers

Furthermore, we find that these are self-similar (power-law) regimes. In the first regime, the interface grows radially and therefore to the power of $1/2$ with time. It is merely expanding as a circle, forming the compact core of the pattern. In the second regime, the interface growth rate increases to a linear one with time. This regime is the one in which the fingers are growing larger and adding extra interface while the core is still expanding. Finally, the fingering pattern enters the last regime, in which the interface growth rate slows back down to a power of $1/2$ with time. In this last regime, the fingers are no longer growing in proportion to the entire fingering pattern, and are referred to as "fixed" fingers because they are not generating additional interfacial length. In fact, there is an equivalent circle that could replace the pattern from this stage on as the interface growth over time is once more simply like that of a solid circle.

This result suggests that viscous fingering only affects the intermediate and last regimes: the fingers affect the interface growth at intermediate times, and affect only the coefficient of scaling at late times, in the sense that there is still an increased interface because of the existence of fingers, but the fingers are no longer actively adding to the growth of the interface.

Chapter 4

Conclusions and Future Work

4.1 Conclusions

In this research, we use a Hele-Shaw cell to investigate experimentally how changing three parameters — the injection rate, the viscosity contrast between the two fluids, and the gap thickness through which the fluid flows — affects the resulting fingering pattern. The results lead to some basic observations, such as finger widths increasing uniformly with gap thickness, or that increasing the mobility ratio leads to more and narrower fingers. Surprisingly, we also observe that by systematically changing only the injection rate at regular intervals, a non-monotonic trend exists for finger widths in these viscous fingering patterns. The finger widths initially decrease as the injection rate increases, but this trend is reversed past a certain point and the fingers grow wider at the upper range of the injection rates tested. This non-monotonicity can also be observed when the dominant wavelength is calculated in a linear stability analysis.

In addition to this, an interface length analysis conducted over time rather than across parameters reveals three power-law regimes that occur over the course of an experiment. The interface growth rate moves through an initial regime of compact radial expansion before fingering, an intermediate regime where there is an accelerated period of interface growth due to fingering, and a final regime of radial expansion with

fixed fingers in which the fingers only affect the coefficient of scaling.

Both of these observations are important as they affect the expected total displacement area when viscous fingering is observed, as well as the total interface available for mixing. Thus, they form the basis of future work in the investigation of the evolution of radial miscible viscous fingering patterns.

4.2 Future Work

One clear area of future work is explaining the cause of the non-monotonic behavior in the dependence of finger width with injection rate. Another is understanding the mechanisms behind when and how the fingering pattern moves through the three different regimes. For both of these questions, it will also be worthwhile to determine whether these three regimes are universal, as the current data only tests for mobility ratios of up to ten.

Finally, an interesting observation that requires further investigation is the formation of a "halo" around each finger that occurs at high injection rates. This is the ring of fainter blue around the darker finger that can be seen in the $Q = 1$ mL/min and $Q = 2$ mL/min fingering patterns of Figure 3-4. Currently, the mechanism behind the formation of this halo is unknown, and the fingering pattern looks significantly different that it is likely a manifestation that a different regime of mixing efficiency can be expected.

Thus, it will be important to pursue these areas of future work in order to develop a better understanding of how miscible viscous fingering patterns evolve, which is critical in being able to accurately determine the volumetric sweep and mixing efficiency of a given fingering pattern.

Bibliography

[1] Ching-Yao Chen, C.-W. Huang, and L.-C. Wang. Controlling radial fingering patterns in miscible confined flows. *Physical Review E*, 82:1–8, 2010.

[2] Ching-Yao Chen, Hermes Huang, C.-W.and Gadêlha, and José A. Miranda. Radial viscous fingering in miscible hele-shaw flows: A numerical study. *Physical Review E*, 78:1–15, 2008.

[3] J.-D. Chen. Radial viscous fingering patterns in hele-shaw cells. *Experiments in Fluids*, 5:363–371, 1987.

[4] J.-D. Chen. Growth of radial viscous fingers in a hele-shaw cell. *Journal of Fluid Mechanics*, 201:223–242, 1989.

[5] Nian-Sheng Cheng. Formula for the viscosity of a glycerol-water mixture. *Industrial and Engineering Chemistry Research*, 47:3285–3288, 2008.

[6] R. L. Chuoke, P. von Meurs, and C. van der Poel. The instability of slow, immiscible, viscous liquid-liquid displacements in permeable media. *Petroleum Transactions*, 216:188–194, 1959.

[7] Gokhan Coskuner. Onset of viscous fingering for miscible liquid-liquid displacements in porous media. *Transport in Porous Media*, 10:285–291, 1993.

[8] G.M. Homsy. Viscous fingering in porous media. *Annual Review of Fluid Mechanics*, 19:271–311, 1987.

[9] Birendra Jha, Luis Cueto-Felgueroso, and Ruben Juanes. Fluid mixing from viscous fingering. *Physical Review Letters*, 106:1–4, May 2011.

[10] L. Paterson. Fingering with miscible fluids in a hele-shaw cell. *Physics of Fluids*, 28(1):26–30, January 1985.

[11] P. Petitjeans, Ching-Yao Chen, Eckart Meiburg, and T. Maxworthy. Miscible quarter five-spot displacements in a hele-shaw cell and the role of flow-induced dispersion. *Physics of Fluids*, 11(7):1705–1716, July 1999.

[12] P. Petitjeans and T. Maxworthy. Miscible displacements in capillary tubes part 1. experiments. *Journal of Fluid Mechanics*, 326:37–56, 1996.

[13] O. Praud and H. Swinney. Fractal dimension and unscreened angles measured for radial viscous fingering. *Physical Review E*, 72:1–10, 2005.

[14] A. Riaz and Eckart Meiburg. Radial source flows in porous media: Linear stability analysis of axial and helical perturbations in miscible displacements. *Physics of Fluids*, 15(4):938–946, April 2003.

[15] P.G. Saffman and G. Taylor. The penetration of a fluid into a porous medium or hele-shaw cell containing a more viscous fluid. *Proceedings of the Royal Society*, 245:312–329, 1958.

[16] Sigma-Aldrich. Erioglaucine disodium salt msds. Technical Report 861146, Sigma-Aldrich, 2012.

[17] Warren C. Young and Richard C. Budynas. *Roark's Formulas for Stress and Strain.* McGraw-Hill, 7th edition, 2002.